

Article

Detection and Statistics of Offshore Aquaculture Rafts in Coastal Waters

Chen Zhou ¹, Kapo Wong ² , Jin Yeu Tsou ^{3,4}  and Yuanzhi Zhang ^{1,3,*}

¹ School of Marine Sciences, Nanjing University of Information Science and Technology, Nanjing 210044, China; 20201209018@nuist.edu.cn

² School of Nursing, The Hong Kong Polytechnic University, Kowloon 999666, Hong Kong; portia.wong@polyu.edu.hk

³ Faculty of Social Science, Center for Housing Innovations and Institute of Asia-Pacific Studies, Chinese University of Hong Kong, Shatin 999077, Hong Kong; jytsou@cityu.edu.hk

⁴ College of Engineering, City University of Hong Kong, Tat Chee Avenue, Kowloon 999077, Hong Kong

* Correspondence: yuanzhizhang@cuhk.edu.hk; Tel.: +86-188-8885-3470

Abstract: Offshore aquaculture is critical for a marine fishery economy. The spatial distribution of aquaculture that characterizes it plays a vital role in the sustainable development of marine resources and the protection of the marine environment. In recent years, China's aquaculture has developed rapidly; specifically, the scale of aquaculture has dramatically expanded, and large-scale aquaculture has gradually grown in popularity. Although high-resolution satellite data can accurately extract aquaculture areas, the extraction of a large area of the sea area requires a copious amount of data. In contrast, medium-resolution satellite images allow for the extraction of aquaculture areas from large sea areas with a smaller amount of data, offering significant advantages. Therefore, we used Landsat8 satellite data to extract and count the number of aquaculture rafts based on the Hough transform and Canny edge detection methods. We tested the accuracy of this method by selecting Haizhou Bay as the study area for the experiment and accuracy verification and found that the automatic extraction accuracy for the number of aquaculture rafts was more than 90%. Additionally, we calculated statistics on the number of aquaculture rafts in Haizhou Bay over the past seven years. The findings presented in this paper offer a significant reference value for local marine utilization, marine environment protection, and marine disaster prevention and mitigation.

Keywords: satellite remote sensing; aquaculture raft; marine environment protection; sustainable development



Citation: Zhou, C.; Wong, K.; Tsou, J.Y.; Zhang, Y. Detection and Statistics of Offshore Aquaculture Rafts in Coastal Waters. *J. Mar. Sci. Eng.* **2022**, *10*, 781. <https://doi.org/10.3390/jmse10060781>

Academic Editors:
Francesco Tiralongo, Caterina Longo and Cataldo Pierri

Received: 3 May 2022

Accepted: 3 June 2022

Published: 5 June 2022

Publisher's Note: MDPI stays neutral with regard to jurisdictional claims in published maps and institutional affiliations.



Copyright: © 2022 by the authors. Licensee MDPI, Basel, Switzerland. This article is an open access article distributed under the terms and conditions of the Creative Commons Attribution (CC BY) license (<https://creativecommons.org/licenses/by/4.0/>).

1. Introduction

As a rapid development in terms of aquaculture, China ranks first in the region and features the highest aquaculture output worldwide [1]. According to data from the UN Food and Agriculture Organization (FAO), over the past three decades, China's aquaculture industry has developed rapidly [2], accounting for more than 60% of the world's aquaculture area and output [3]. According to the *Chinese Fishery Statistics Yearbook*, the output value of aquaculture in China during 2019 was CNY 357.53 billion, while the aquaculture output was 20.65 million tons, and Chinese aquaculture occupied an area of 1.99 million hectares [4]. The main aquaculture method employed—raft cultivation in a shallow sea area—has expanded rapidly due to the fact of its high economic output value and high return [5]. Although this industry is currently making significant contributions to the supply of aquatic products, it is also characterized by various problems such as poorly planned distribution of aquaculture and blind expansion [6]. Economic interests have driven the uncontrolled development of many aspects of raft culture, entering a disorganized stage of development; on the basis of the blind construction of structures and breeding rafts, the breeding density has become too high, far beyond the capacity of

the marine ecosystem, causing a disruption in it and the natural energy cycle [7–9]. At the same time, aquaculture has negative impacts in the form of decomposing residual materials, debris, and fish and shrimp excrement, along with household garbage from aquaculture workers. All of these factors produce large amounts of nonprotein nitrogenous substances and phosphorus nutrients waste products, leading to the eutrophication of water, resulting in a decrease in water quality and serious damage to the ecology of coastal areas [10–12]. Moreover, a large number of metal rafts produce heavy metal pollution, which is harmful to human health [13]. Therefore, unplanned raft aquaculture is gradually becoming a critical source of pollution in offshore waters, even exceeding land-based pollution. Consequently, large-scale offshore raft farming areas have been subject to the greatest damage from marine disasters [14,15], as frequent typhoons, storm surges, and other marine disasters in recent years have also caused a non-negligible impact on offshore farming areas, seriously affecting the healthy and sustainable development of the social economy in coastal areas [16]. Therefore, conducting a large-scale statistical analysis of offshore raft culture areas is particularly necessary. When engaging in scientific planning of aquaculture areas to achieve sustainable and healthy development, the collection and analysis of relevant regional data connecting aquaculture can help mitigate and defend against natural disasters [17].

Due to the limits in terms of manpower and material resources, monitoring large-scale raft aquaculture areas is difficult when using traditional onsite investigation methods. However, satellite remote sensing represents an increasing mature earth observation technology that has made up for the shortcomings of traditional survey methods with features such as wide coverage, all-weather capability, and strong synchronization. Thus, this technological tool is playing an increasingly vital role in monitoring aquaculture areas [18]. Performing rapid extraction and calculation of statistics on seawater raft aquaculture areas using satellite images is of great social and economic value with practical significance, and it can be employed to conduct statistical research encompassing large-scale aquaculture area data [19].

Seawater is the background of offshore aquaculture operations, and the surrounding land features are relatively uniform. Researchers have achieved specific effects by applying many methods of extracting aquaculture areas using high-resolution images. For example, Zhang et al. proposed an accurate segmentation method for high-resolution remote sensing images [20]. According to the multistage and multiscale segmentation model, through the identification and fusion of meaningful paths between different levels, the purpose of segmentation accuracy optimization was obtained, and the subsequent optimization of segmentation had the greatest potential [20]. Jiang et al. described a method to optimize the cross-entropy loss function via a uniformly distributed disturbance term that the scholars constructed to optimize the model using GF-2 series remote sensing image data and a 3D-CNN neural network. According to their findings, the neural network model was suitable for the extraction of large-scale and multitemporal aquaculture areas [21]. Wang et al. applied the original regional line segment association framework (RLPAF) to a study of aquaculture areas with high-resolution images through a method based on object analysis. The researchers suggested that the extraction of aquaculture rafts using high-resolution remote sensing images, based on multiscale feature fusion and regional association, offered obvious advantages over ordinary object-based image analysis methods [22]. Cheng et al. tested an HDCU net threshold segmentation network based on HDC and U-NET. They used GF-2 satellite images as experimental data to extract breeding areas and compared the data with four other threshold segmentation methods to verify the effectiveness of this method [23]. Overall, high-resolution satellite imagery used to examine aquaculture has a higher extraction accuracy. Moreover, the extraction of culture zones on a small-scale sea area has shown good performance in practical terms. However, the extraction of a large area of seawater involves various difficulties. For example, applying high spatial resolution in a large area of water requires much data splicing of remote sensing data. Furthermore,

the huge amount of data involved in analyzing a large sea area also increases the difficulty of practical operation.

The resolution of satellite data used to extract a large area of water featuring breeding raft technology has a more considerable superiority. King and others used NDVI and edge detection in remote sensing image spectral and spatial characteristics in the extraction of seawater culture zones and compared it with the effect of pure culture zone recognition. The method, which obviously improved extraction accuracy for complex water culture zones, has excellent potential for the rapid extraction of large aquaculture areas [24]. Liu et al. applied an unsupervised classification algorithm to classify and extract China's offshore raft aquaculture and cage aquaculture and calculated statistics on the proportion of China's offshore aquaculture area in each province. The authors used high-resolution images to test the accuracy of the results. This technique now plays a vital role in China's aquaculture planning and ecological environmental protection [25]. Lu et al. used an object-oriented extraction method to analyze the spatial distribution of laver cultivation in the Lianyungang Sea area over the previous 15 years and discussed the transfer direction and distance of cultivation in three different regions to facilitate the management of laver cultivation areas [26]. At present, satellite image resolution based on the spectral ratio method is used for the extraction of seawater culture zones for large areas, such as breeding raft farms that are mainly distributed in estuary and coastal bay waters, where the sea background is relatively complex. Around culture zones, the level of chlorophyll and the sediment content are higher. Thus, the sea spectrum, to a certain degree, facilitates a reducing influence of the extraction accuracy [27].

The previously described methods used medium- and high-resolution satellite data to extract the spatial distribution of aquaculture areas and achieved many results. For large areas of sea aquaculture raft number statistical calculations, few people are involved. In the interest of facilitating rapid statistical analysis of the number of raft farming areas, this paper proposes an approach involving automatic extraction and statistical calculations for raft farming areas based on the fusion of edge detection and the Hough transform. The new method uses medium-resolution satellite images. First, we applied edge detection technology and incorporated the spatial characteristics of the aquaculture rafts in remote sensing images to extract the aquaculture areas. This technique avoided the complex spectral characteristics of a large sea area in improving the aquaculture rafts' extraction accuracy. Visual interpretation was used to evaluate the accuracy of the data, yielding an overall accuracy of over 90%. Moreover, this study was the first to use medium-resolution satellite data to automatically count the number of aquaculture rafts in a large area [28].

2. Materials and Methods

2.1. Study Area and Aquaculture Raft Data

Raft farming in Asia accounts for more than 90% of the world's total [29,30]. In Shandong and Jiangsu provinces, China, raft farming has a large area and relatively high yield, impacting the environment. Haizhou Bay, located to the east of Lianyungang, Jiangsu Province, has suitable natural conditions, a superior environment, and developed aquaculture. Therefore, this paper selected the aquaculture area of Haizhou Bay in Lianyungang, Jiangsu Province, China, as the study area for the statistical calculation of the number of aquaculture rafts (Figure 1).

In the paper, Landsat 8 OLI image data were selected to detect the coastal breeding rafts in the study area. The image data were obtained from the United States Geological Survey (<http://glovis.usgs.gov/>, accessed on 7 July 2021). Specific image data are shown in Table 1 in which the five selected areas are all Landsat 8 OLI images available in Haizhou Bay from 2013 to 2020. The image data in areas 1, 2, and 3 were used to extract breeding rafts and for accuracy verification of the statistical calculation of the aquaculture rafts, while the image in areas 4, and 5 were employed to analyze dynamic changes in aquaculture rafts from 2013 to 2020.

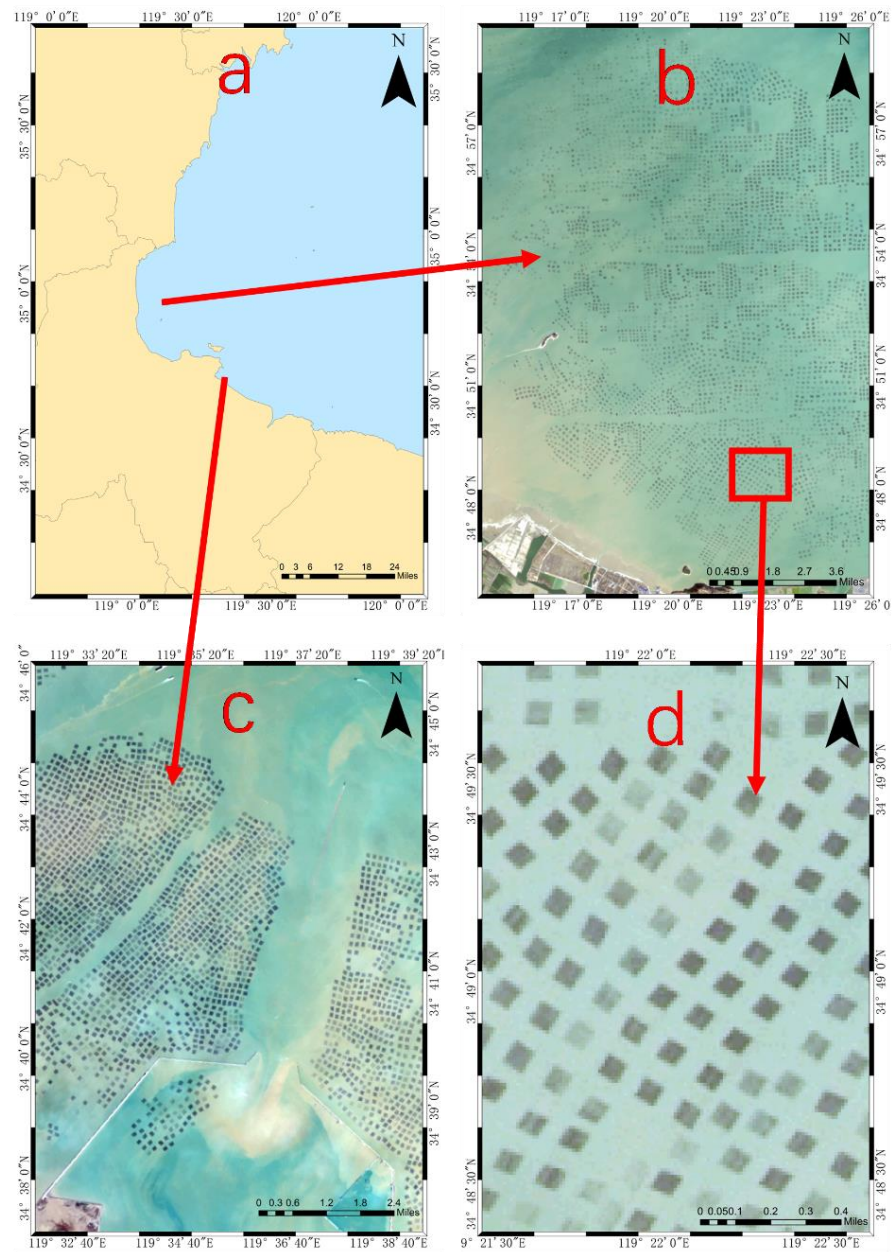


Figure 1. Map of (a) the coverage of the experimental area and aerial photographs of the research areas (b–d); (b–c) images of aquaculture rafts at different locations in Haizhou Bay; (d) a local image of the breeding area.

Table 1. Introduction to the study areas.

Name	Date	Image Path/Row
Area 1	16 January 2019	120,036
Area 2	04 February 2020	120,036
Area 3	04 Decemebr 2020	120,036
Area 4	01 Decemebr 2013	120,036
Area 5	09 February 2016	120,036

2.2. Processing Methods

The new method mainly included the following steps (as shown in a technical flow chart in Figure 2): Step 1—preprocessing of the satellite data including data fusion and water and land separation; Step 2—extraction of the aquaculture area by edge detection

technology; Step 3—using Hough transform technology, processing of the image after edge detection, and through threshold optimization and adjustment, the extraction and automatic statistics of the identification graph (aquaculture raft) are realized, and the number of aquaculture areas is obtained through the automatic statistics of the chart.

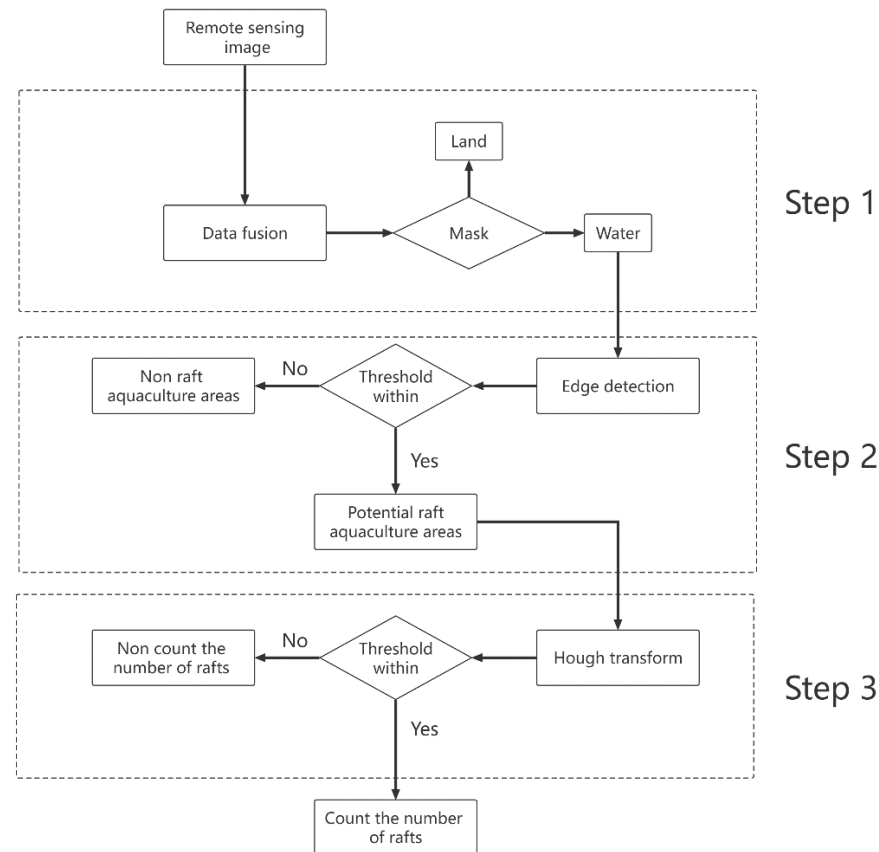


Figure 2. Workflow of the study.

2.2.1. Data Preprocessing

This study employed cloud-free Landsat8 L1 images with medium-resolution for the study area in 2013, 2016, 2019, and 2020. Table 1 provides more data regarding the images.

Different from other methods used to extract cultured areas based on the difference between cultured areas and seawater NDVI, the extraction of aquaculture areas in this study did not need the use of characteristics of the NDVI; thus, the atmospheric correction of images was not required. As the Landsat8 L1 data were geometrically corrected before release, data preprocessing in this study mainly involved data fusion. In other words, more accurate and rich synthetic image data could be obtained by processing images of various resolutions. In this paper, the resolution of the Landsat8 multispectral band was 30 m and that of the panchromatic band was 15 m. To further improve the extraction accuracy of aquaculture areas, the data fusion method was used to combine images at the pixel level while ensuring the spectral information to enhance the image effect and facilitate image feature extraction. In this study, the multispectral and panchromatic band images were fused by ENVI's Gram–Schmidt method to improve the spatial resolution of the multispectral band remote sensing images [31].

2.2.2. Land and Water Separation

For the remote sensing images' land and water separation, we mostly relied on the green band with other band ratio indexes, namely, the normalized difference water index (NDWI) and modified normalized difference water index (MNDWI) with water extraction [32,33]. For some land images, there exist more rivers, ponds, small areas of land,

and other water bodies in the image, and the utilization ratio of the index of the marine and land separation effect was poor. The accurate extraction of ocean water could not be achieved. Therefore, we used the mask method and ENVI software to accurately cut the sea water area, eliminating the background image of land, separating the ocean water body from the land, and accurately extracting the sea water areas.

2.2.3. Extraction of Raft Aquaculture Areas

The edge detection algorithm can be used to detect the edges of objects in images and recognize the edges of aquaculture rafts. An extraction diagram of a raft breeding area based on edge detection is shown in Figure 3. First, the edge features of the image were extracted from the original image, and the edge was recorded as a two-dimensional matrix, where the edge was one and the background was 0. The algorithm was used to fuse the edge feature image with the original image to obtain a satellite image marked by the edge feature [34,35]. The details of these steps are outlined below.

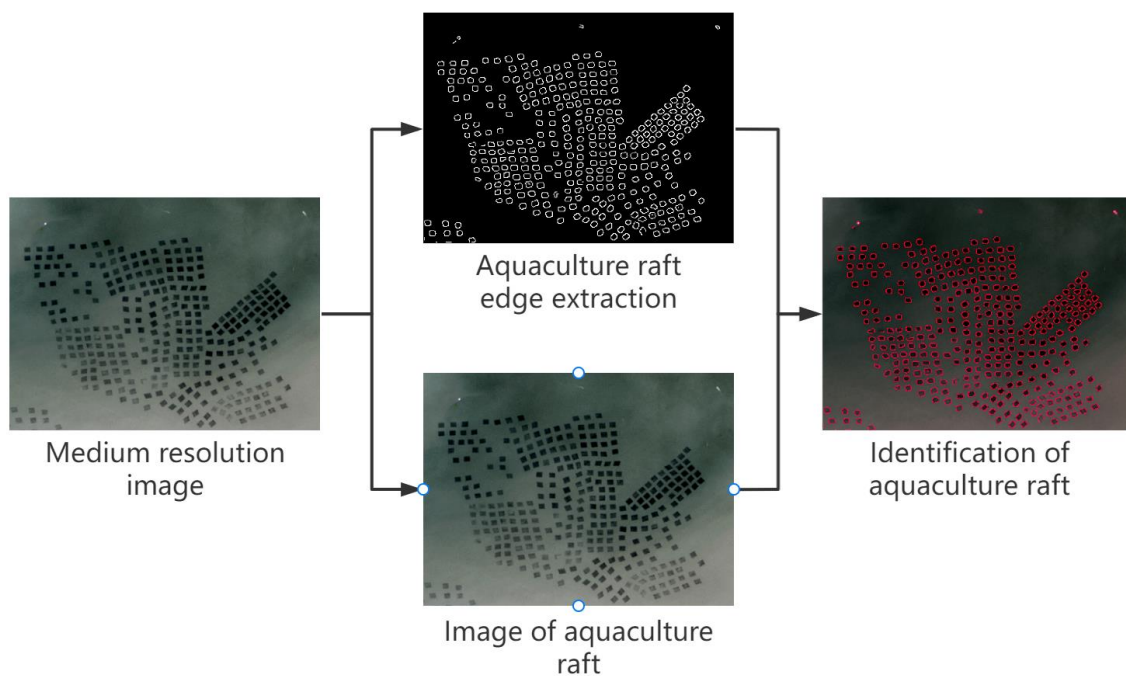


Figure 3. Extraction diagram of the culture area.

The edge detection algorithm used in this study was the Canny operator, which is an edge detection algorithm, implemented by John in 1986, with a multistage wide spectrum algorithm [36]. The main flow is shown in Figure 3.

In the first step, the Gaussian filter convolved with the image. The Canny operator is susceptible to noise, and Gaussian blur was used to reduce the influence of noise so as to prevent noise in the image of the edge detection results [26]. The function is expressed as:

$$H(x, y) = \frac{1}{2\pi\sigma^2} \exp\left(-\frac{x^2 + y^2}{2\sigma^2}\right) \tag{1}$$

where (x, y) represents the coordinates of the pixel points, and σ represents the distribution parameters of the Gaussian filter. The smaller σ is, the smaller the noise suppression ability and the higher the precision of the edge positioning. The value of σ determines the effect of image denoising.

In the second step, the Sobel operator was used to calculate the first derivative of horizontal and vertical directions, namely, the image gradient $(G_x$ and $G_y)$, to process the

smoothed image further. The gradient and direction of the boundary can be calculated as follows:

$$G_x(i, j) = \frac{[I(i, j + 1) - I(i, j) + I(i + 1, j + 1) - I(i + 1, j)]}{2} \tag{2}$$

$$G_y(i, j) = \frac{[I(i, j) - I(i + 1, j) + I(i, j + 1) - I(i + 1, j + 1)]}{2} \tag{3}$$

where $I(i, j)$ is the gray value at point (i, j) . The gradient value $G(i, j)$ at point (i, j) and the gradient direction $\theta(i, j)$ are:

$$G(i, j) = \sqrt{G_x^2(i, j) + G_y^2(i, j)} \tag{4}$$

$$\theta(i, j) = \arctan\left(\frac{G_y(i, j)}{G_x(i, j)}\right) \tag{5}$$

After obtaining the magnitude and direction of the gradient, the whole image was scanned, and the non-boundary points were removed; that is, 0 was set. By scanning each pixel, we determined whether it was the most prominent point in the same gradient direction around it.

In Step 4, to further determine the boundary, two thresholds (i.e., low threshold (TL) and high threshold (TH)) need to be set for boundary judgment. When the gray value of the image is lower than TL, the value higher than TH is considered as the image boundary. When the gray value is between the two, if the point is connected to the real boundary point, it is considered as the boundary. This paper calculated the TL and TH boundaries according to the percentage of non-edge pixels in total pixels and the ratio of high and low thresholds.

2.2.4. Number of Aquaculture Raft Extraction

A raft farming area can be accurately identified in remote sensing images through the edge detection method used above. An obviously closed graph is formed at the edge of each farming raft, as shown in Figure 4. In this paper, based on the Hough transform principle and the advantages of the high efficiency, high speed, and low cost of machine vision, the Hough transform algorithm parameters were optimized to identify the closed graph in Figure 4. Depicted as circles, and automatically counting the number of circles [37], the number statistics of aquaculture rafts is realized. Hough transform is mainly used in computer vision to transform spatial detection into the problem of parameter space through the point–line duality of image space and parameter space [38–41], which is widely used in computer vision.

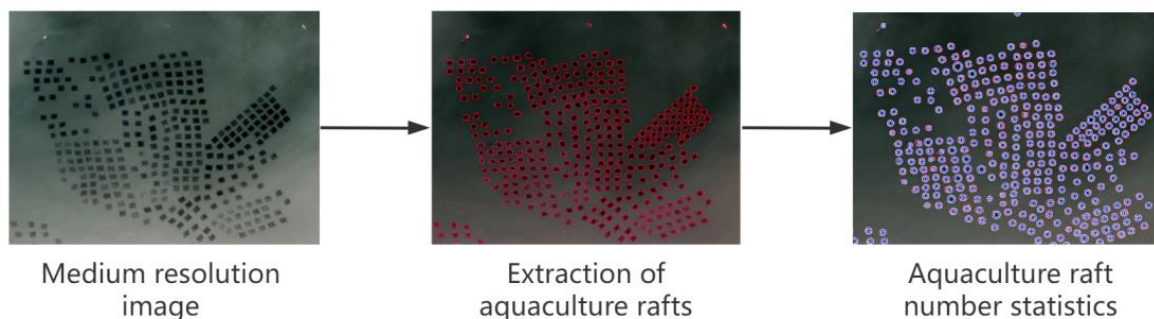


Figure 4. Schematic diagram of the automatic statistics of the aquaculture rafts.

The basic idea of the Hough transform circle detection is to map the edge pixels in the image space to the parameter space, accumulate the corresponding cumulative values of coordinate point elements in the parameter space, and finally determine the center and radius of the circle according to the cumulative values [42].

The general equation of a circle can be written as:

$$(x - a)^2 + (y - b)^2 = r^2 \quad (6)$$

where (a, b) is the center of the circle, and r is the radius. In the Cartesian coordinate system, the point (x, y) on the circle is converted to the polar coordinate plane, and the corresponding formula is:

$$\begin{cases} x = a + r \cos \theta \\ y = b + r \sin \theta \end{cases} \quad (7)$$

Suppose an edge point (x_0, y_0) in the image space maps to the parameter space with radius r_0 . Substitute the edge point (x_0, y_0) into (7) and then perform the corresponding transformation, which can be written as:

$$\begin{cases} a = x_0 - r_0 \cos \theta \\ b = y_0 - r_0 \sin \theta \end{cases} \quad (8)$$

when $\theta \in [0, 2\pi)$ is traversed, the point (x_0, y_0) in the image space is mapped to the shape of the parameter space as a circle. Therefore, every edge point in the image space corresponds to the parameter space as a circle.

If four edge pixel points, A, B, C, and D, are extracted from the remote sensing images and mapped to the parameter space with radius R, it can be seen from the figure that each point in the image was mapped to the parameter space as an A circle. The four circles in the parameter space intersect at the O point. The point with the maximum cumulative value in the parameter space was found through the statistics of coordinate points in the parameter space. In the case of the determination of radius, it can be seen that the cumulative value of point O was the largest in the parameter space, which is also the center of the circle in the image space.

In the operation of this paper, the radius of the detection circle was used as the threshold value. By setting the upper and lower limits of the detection circle's radius, the extraction of breeding areas can be further accurately achieved. Then, the point (x, y) in the remote sensing image is mapped to the parameter space (a, b, r) , and any point in the image corresponds to a conical surface in the parameter space. In this way, the detection of the circle changes from two-dimensional to three-dimensional. Since r has a threshold limit, the mapping to the parameter space is a roundtable. Multiple circles intersect at a point (a_0, b_0, c_0) , reflecting the circle's coordinates and radius. In circle recognition, we can find the center and radius by calculating the maximum cumulative value and then marking all circle pixels through traversal.

The number of circles, namely, the number of raft breeding areas, can be obtained automatically by calculating the center of circles detected by the Hough transform.

2.3. Threshold Setting

According to the description in the second part, the method in this paper mainly involved three thresholds, which were the setting of the high and low thresholds of edge detection and the threshold setting in the Hough transform detection.

In the use of edge detection in the process of the recognition of raft culture zones, due to the influence of ocean waves and other image characteristics, it is easy to cause ocean waves to exist in the process of edge detection and image noise interference by setting the detection threshold too small, easily causing breeding raft leak identification, leading to extraction that is not comprehensive. If the detection threshold is too large, it easily causes the false recognition of noise such as waves and ripples [43]. Therefore, choosing appropriate high and low detection thresholds can ensure that the raft breeding area can be accurately identified, eliminating the interference of other noises.

The Hough transform also plays a key role in threshold size control during the detection of the closed graph. If the threshold scale is set too large, it easily identifies multiple aquaculture rafts as a single one, resulting in a small statistical number. If the threshold

scale is set too small, it is easily identifies more than one aquaculture raft, or the image noise is mistakenly identified as an aquaculture raft, resulting in the number of automatic statistics being greater than the actual number of aquaculture rafts. Therefore, the correct setting of the threshold values in the Hough transform process can ensure that each aquaculture raft is identified as a figure and counted in the quantity statistics.

3. Results

Figures 5–7 and Table 2 show the results of using edge detection algorithms for the relatively accurate identification of breeding rafts when waves did not exist. During calm seas, the water provides a relatively homogeneous background, and through the setting of thresholds, using edge detection to identify more accurate aquaculture zones, there was almost no deterrent to other phenomena. In the case of a large sea area, the seawater background is relatively complex. For example, features, such as waves and ships on the sea surface, may introduce noise, leading to the phenomenon of misidentifying other types in edge detection. In comparison, NDVI and other texture features rely on the spectral difference between seawater background and aquaculture area to identify aquaculture areas. In this context, the influence of algae chlorophyll, suspended sediment, and other factors may lead to spectral similarity between aquaculture areas and seawater background, resulting in a higher extraction error recognition rate for aquaculture areas. Using the spatial characteristics of remote sensing images for edge recognition, as well as using the difference in pixel gradients for extraction and recognition of aquaculture areas, this significantly reduces or prevents a large false recognition rate caused by the similarity between aquaculture areas and parts of the seawater background spectrum.

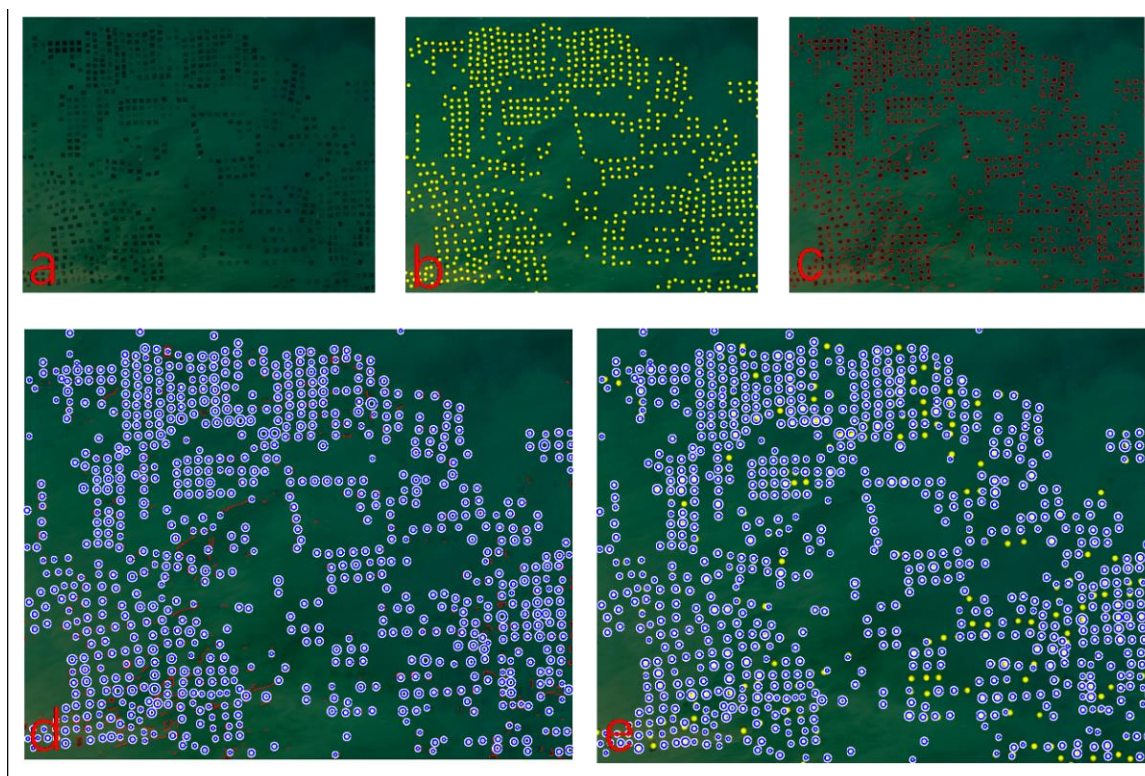


Figure 5. Experimental results in study area 1: (a) original image; (b) visual interpretation results; (c) identification results; (d) quantitative identification results; (e) overlap between the quantitative identification results and the visual interpretation results.

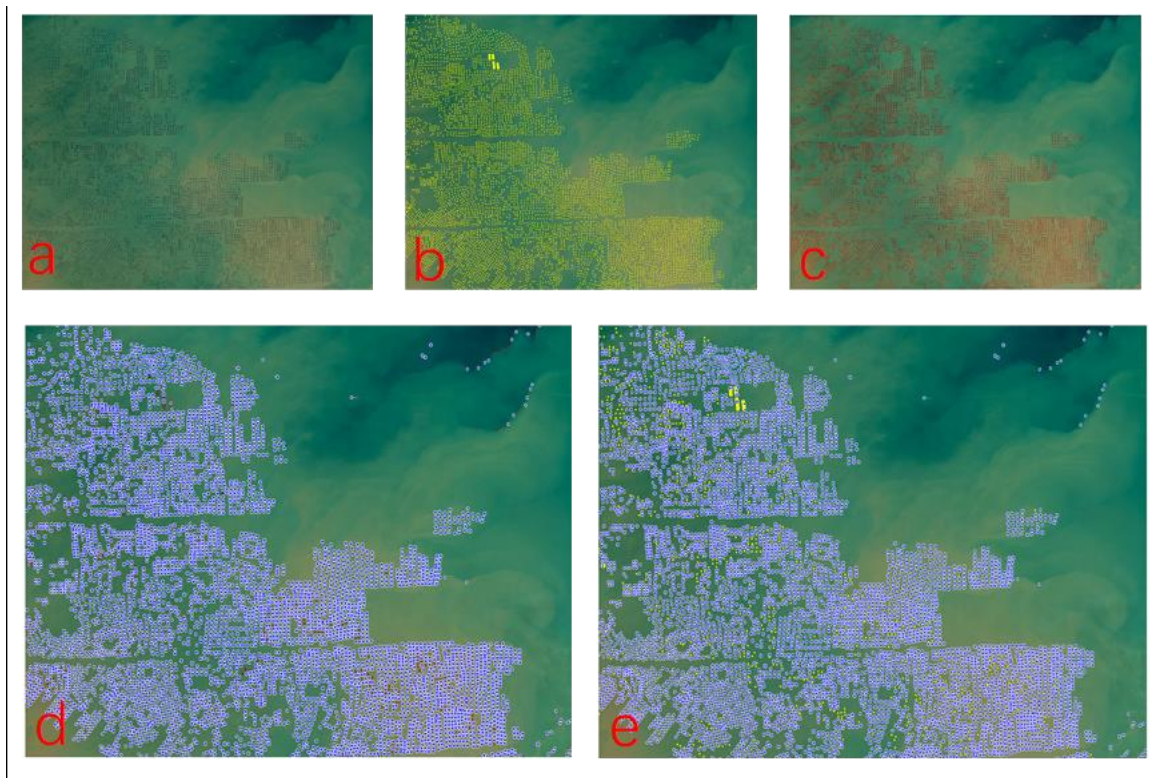


Figure 6. Experimental results in study area 1: (a) original image; (b) visual interpretation results; (c) identification results; (d) quantitative identification results; (e) overlap between the quantitative identification results and the visual interpretation results.

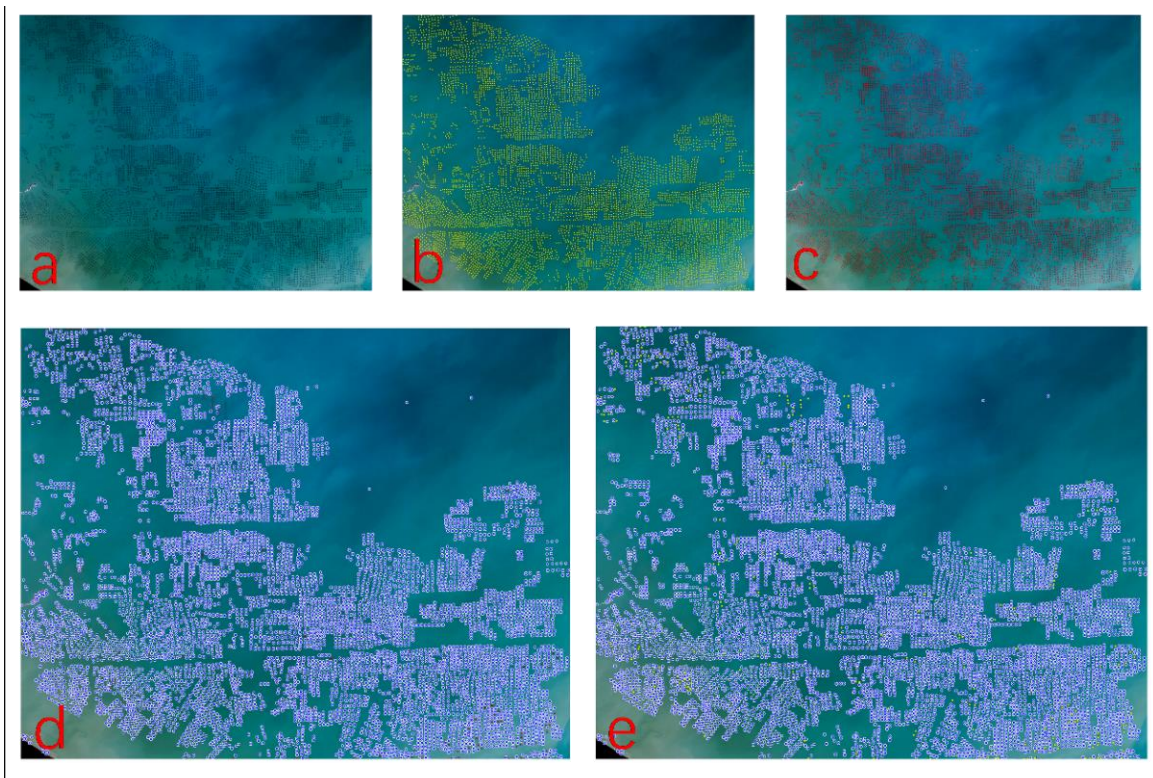


Figure 7. Experimental results in study area 1: (a) original image; (b) visual interpretation results; (c) identification results; (d) quantitative identification results; (e) overlap between the quantitative identification results and the visual interpretation results.

Table 2. Accuracy evaluation results of three different experimental areas.

Research Area	Extraction Quantity	Precision	FAR	MAR
Research Area 1	730	92.21%	2.19%	7.79%
Research Area 2	5753	90.23%	0.75%	9.77%
Research Area 3	6879	92.98%	0.78%	7.02%

In the remote sensing image processed by the edge detection algorithm, the aquaculture raft in the image was characterized by an obvious edge, which proved convenient for identifying aquaculture rafts using the Hough transform. Nevertheless, in comparison to the identification of aquaculture rafts by edge detection, using the Hough transform principle to count the number of aquaculture rafts automatically involved a certain amount of misidentification and omission due to the uncertainty of the results introduced in the previous step.

As can be seen from the diagram, using the Hough transform method for processing images marginalized characteristics, the recognition of breeding rafts supported the calculation of accurate and automatic statistics, and for the ocean waves of edge detection in the process of information, such as noise using the Hough transform, can also further filter accurately.

This paper also identified aquaculture rafts in the whole sea area of Haizhou Bay. According to the changes in sea area covered by aquaculture rafts, as shown in Figure 8a–c, and in different years and statistical calculations, as shown in Figure 9, it can be seen that from 2013 to 2020, the aquaculture area and the number of aquaculture rafts in Haizhou Bay of Lianyungang increased rapidly, from more than 3000 aquaculture rafts in 2013 to more than 6000 rafts in 2016 and reaching nearly 12,000 rafts by 2020.

For small area waters, as shown in Figure 4, automatic identification using the method described here was utilized to extract basic shapes that could render precise statistics on the number of breeding rafts. Because of the uncertainty in each step that was introduced as a result, this automatically led to a decline in identify extraction accuracy and the number of breeding rafts over a large area of water, despite a certain amount of error identification and omissions. However, the accuracy rate was above 90%, confirming the effectiveness of the automatic identification and the statistical method related to the number of aquaculture rafts over a large sea area.

The most commonly used accuracy evaluations include accuracy rate, false alarm rate, and missed alarm rate. Equations (9)–(11) were used to evaluate the accuracy [17]:

$$Precision = \frac{TQ - FN}{TQ + FQ - FN} \quad (9)$$

$$FAR = \frac{FN}{TQ} \quad (10)$$

$$MAR = \frac{FQ}{TQ + FQ - FN} \quad (11)$$

where FQ is the number of unextracted aquaculture rafts, FN is the number of incorrectly extracted aquaculture rafts, TQ is the number of automatically extracted aquaculture rafts by this method, $TQ - FN$ is the number of correctly extracted aquaculture rafts by this method, and $TQ + FQ - FN$ is the real number of aquaculture rafts.

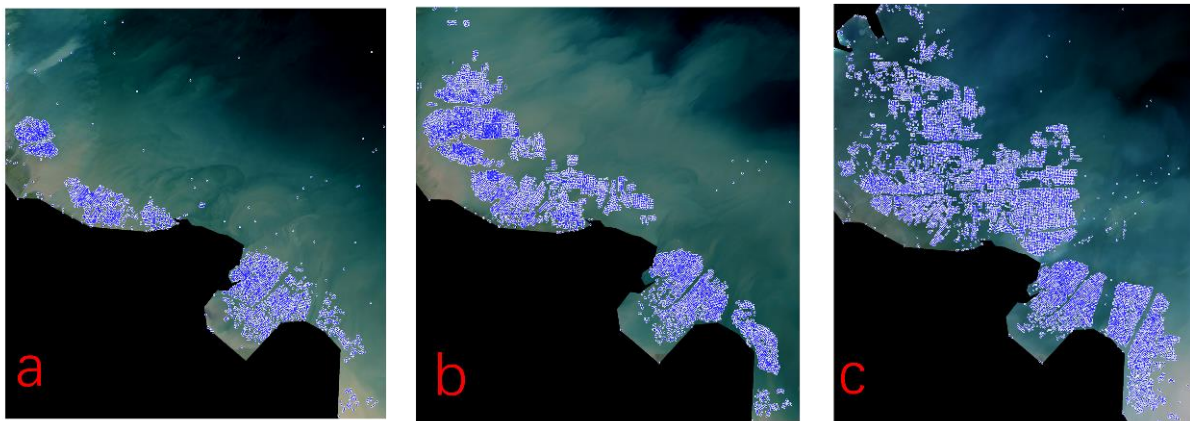


Figure 8. Haizhou Bay aquaculture zones: (a) 2013; (b) 2016; (c) 2020.

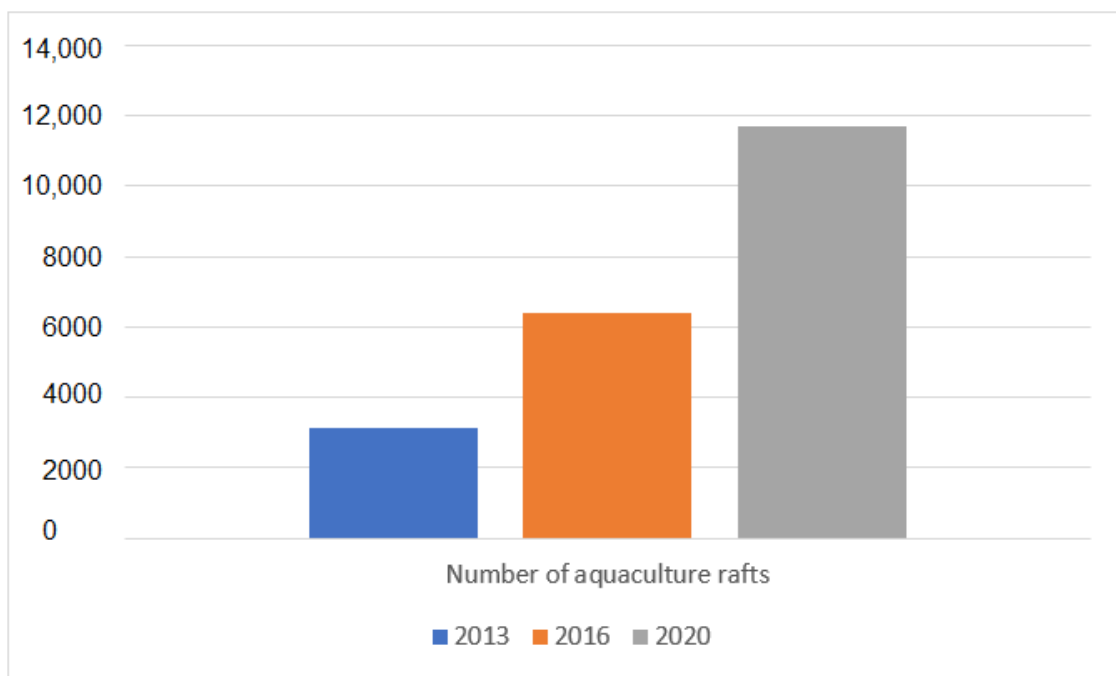


Figure 9. The quantity changes in aquaculture rafts in Haizhou Bay.

4. Discussion

Based on the above method and accuracy verification, we identified and counted aquaculture rafts in the whole sea area of Haizhou Bay. Because chlorophyll is concentrated in raft culture, there are also predecessors using NDVI to extract aquaculture raft [33]. However, extensive coastal raft culture is easily confused with the heterogeneous water background. This results in unsatisfactory extraction when surveying a large water area with a heterogeneous water background [44]. For the use of general object-based supervised classification to achieve extraction, the selection of a large number of samples during the training stage when the background water area is heterogeneous is also required [45–47]. This paper was based on edge detection and Hough transform, and it identified and counted aquaculture rafts in the whole sea area of Haizhou Bay. It can be seen that in the sea area of Haizhou Bay, where the water background was relatively complex, the method in this paper avoided the characteristic of a complex optical background of a large water area and achieved the identification and statistics of aquaculture rafts over a large area (Figure 8).

As can be seen from Figure 8, in the face of the optical background sea area loaded in Haizhou Bay, the algorithm in this paper achieved the accurate identification and statistics

of aquaculture rafts and achieved the purpose of monitoring the aquaculture area. However, the presence of ships and relatively obvious waves on the sea surface generated noise in the process of remote sensing image recognition and extraction, as shown in Figure 10. Thus, sporadic misidentification occurred on the sea surface without aquaculture areas, which can be explained by the fact that the ships' and waves' spatial characteristics and sizes were similar to that of aquaculture rafts.

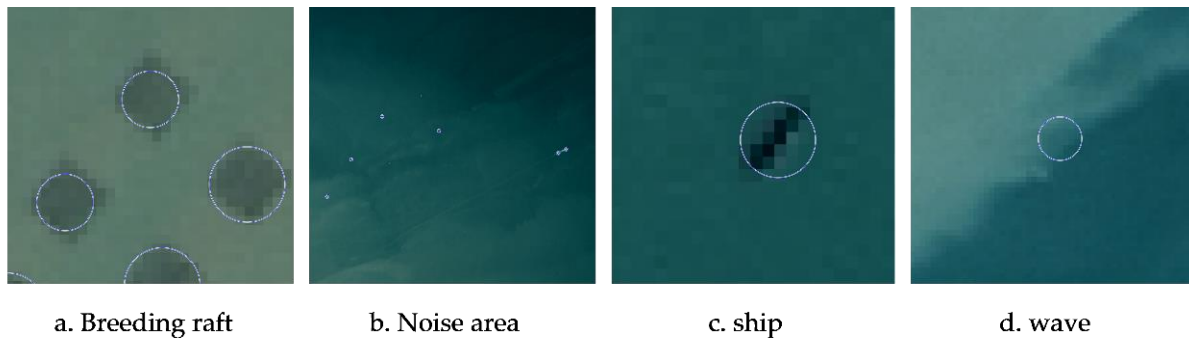


Figure 10. Local noise region: (a) identified aquaculture rafts; (b) noise identified on the sea surface; (c,d) noise caused by ships and waves.

Figure 11 shows local area diagrams of the extraction statistics of aquaculture rafts from satellite data acquired in 2016. Observably, the method presented in this paper was able to improve the accuracy of the identification, extraction, and quantification of aquaculture rafts from medium-resolution satellite data by using edge detection and Hough transform technology. It can also be seen from Figure 11b that very few aquaculture rafts with obscure edge features could not be correctly extracted because their spatial characteristics too closely resembled the seawater background, resulting in the omission of automatic statistics. For the vast majority of aquaculture rafts, their spatial characteristics could be used for successful extraction.

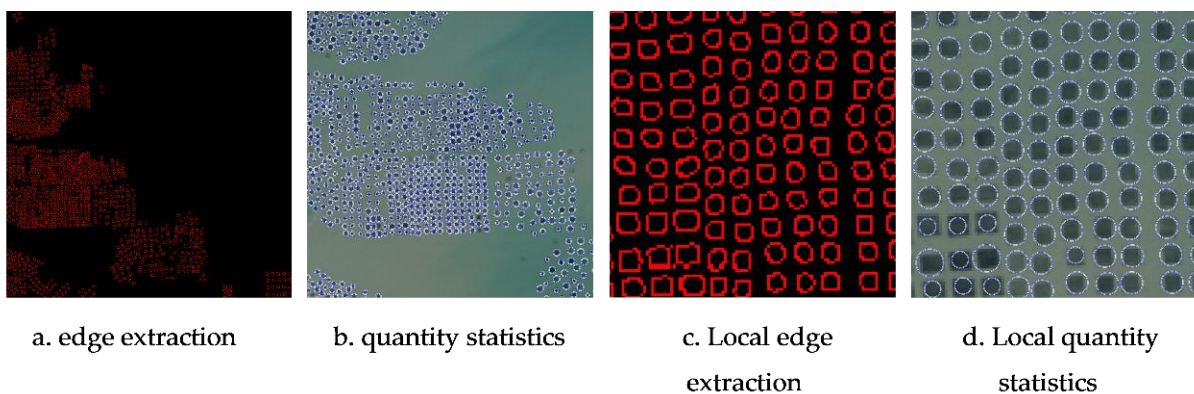


Figure 11. Local renderings of aquaculture raft extraction statistics: (a,b) the results of the identification and extraction of aquaculture rafts on the sea surface, respectively; (c,d) partial displays of extracted statistical results.

As can be seen from the statistical chart of the number of aquaculture rafts in Figure 9, between 2013 and 2020, the number of rafts increased by almost 10,000. Moreover, the number of rafts in 2020 was approximately four times that of laver rafts in 2013. The large-scale growth of laver rafting has had a noticeable promotional effect on the “laver economy” in Lianyungang’s coastal area, driving the development of locally related industries and increasing residents’ income. However, an immense area of growth in local laver cultivation may lead the number of rafts to increase in unsustainable quantities.

Negative factors include the possibility of illegal construction and unsystematic development and breeding, leading to an increasingly serious ecological impact on the sea area of Haizhou Bay. First, the laver cultivation raft provides an ideal attachment place for *enteromorpha prolifera* and other green algae. After the annual harvest of laver, the large number of cultivation rafts increases the possibility of *enteromorpha prolifera* attachment growth and outbreak. Second, seaweed cultivation involves marine plants absorbing nutrients from seawater, which can effectively reduce eutrophication. Therefore, during its growth phase, seaweed can remove a large number of nutrients, such as nitrogen and phosphorus, from the water environment, reducing the likelihood of a green-tide disaster. In this way, the massive growth of breeding raft farming in recent years has also played a particularly positive role in the marine ecological environment.

5. Conclusions

In this investigation, Landsat-8 satellite images were used to study aquaculture rafts in Lianyungang. A method that combined the edge detection and Hough transform technology was adopted to carry out statistical research involving the automatic identification and extraction of aquaculture rafts, and the accuracy of the automatic statistical results was verified by visual interpretation of the remote sensing imagery as the truth value. This method was able to extract and count the number of aquaculture rafts accurately, avoiding the error caused by manual calculation or subjective estimation based on local aquaculture data. The regularity of the shape of the rafts could be used to calculate the area of rafts according to the number of rafts. This paper also applied the method to the images in 2013, 2016, and 2020, identifying laver breeding rafts changes from 2013 to 2020 in Haizhou Bay to statistically calculate laver rafts, and found that the laver breeding raft number increased four-fold over seven years, probably inducing, to a certain degree, the rapid growth in the number and volume of raft frames and the *enteromorpha* disasters that occurred there. Interestingly, meanwhile, increasing the cultivation quantity of laver during its growth cycle can effectively reduce the eutrophication of seawater and positively affect the ecological environment of the sea area.

This method had the following limitations: (1) For the threshold used in this paper, manual adjustment was required to optimize the threshold size to match the appropriate threshold. (2) At present, the calculation of the number of aquaculture rafts in this method is only applicable to aquaculture rafts with a relatively regular and uniform appearance. Thus, further study is needed to investigate methods for calculating the number of aquaculture areas with different types of mixed farming. (3) For the noise phenomena generated by ships and waves on the sea surface, it remains necessary to distinguish the spatial characteristics of ships and aquaculture rafts through follow-up studies to eliminate noise interference. According to these deficiencies, reducing environmental noise and statistically calculating the number of different types of aquaculture rafts is a promising topic for future studies.

Author Contributions: Conceptualization, C.Z. and Y.Z.; methodology, K.W.; software, J.Y.T.; validation, C.Z., K.W. and Y.Z.; formal analysis, C.Z.; investigation, C.Z.; resources, J.Y.T.; data curation, C.Z.; writing—original draft preparation, C.Z. and K.W.; writing—review and editing, Y.Z. and J.Y.T.; visualization, K.W.; supervision, Y.Z.; project administration, Y.Z.; funding acquisition, Y.Z. All authors have read and agreed to the published version of the manuscript.

Funding: This research was funded by the Marine Special Program of Jiangsu Province in China (JSZRHYKJ202007), the National Natural Science Foundation (U1901215), and the Natural Scientific Foundation of Jiangsu Province (BK20181413).

Institutional Review Board Statement: Not applicable.

Informed Consent Statement: Not applicable.

Data Availability Statement: Not applicable.

Acknowledgments: The Landsat 8 OLI images and in situ measurements were highly appreciated. This research was also funded partially by the National Natural Science Foundation (U1901215), the Marine Special Program of Jiangsu Province in China (JSZRHYKJ202007), and the Natural Scientific Foundation of Jiangsu Province (BK20181413).

Conflicts of Interest: The authors declare no conflict of interest.

References

- Xu, J.; Han, L.; Yin, W. Research on the ecologicalization efficiency of mariculture industry in China and its influencing factors. *Mar. Policy* **2022**, *137*, 104935. [[CrossRef](#)]
- Cao, L.; Naylor, R.; Henriksson, P.; Leadbitter, D.; Metian, M.; Troell, M.; Zhang, W. China's aquaculture and the world's wild fisheries. *Science* **2015**, *347*, 133–135. [[CrossRef](#)] [[PubMed](#)]
- Liang, Y.; Cheng, X.; Zhu, H.; Shutes, B.; Yan, B.; Zhou, Q.; Yu, X. Historical Evolution of Mariculture in China During Past 40 Years and Its Impacts on Eco-environment. *Chin. Geogr. Sci.* **2018**, *28*, 363–373. [[CrossRef](#)]
- Zheng, H.; Li, J.; Zhao, X. How does financial policy support the development of China's fishery? Characteristics, experience and prospects. *Mar. Policy* **2021**, *132*, 104678. [[CrossRef](#)]
- Trujillo, P.; Piroddi, C.; Jacquet, J. Fish Farms at Sea: The Ground Truth from Google Earth. *PLoS ONE* **2012**, *7*, e30546. [[CrossRef](#)]
- Li, X.Y.; Yu, R.C.; Geng, H.X.; Li, Y.F. Increasing dominance of dinoflagellate red tides in the coastal waters of Yellow Sea, China. *Mar. Pollut. Bull.* **2021**, *168*, 112439. [[CrossRef](#)]
- Cui, B.; Fei, D.; Shao, G.; Lu, Y.; Chu, J. Extracting Raft Aquaculture Areas from Remote Sensing Images via an Improved U-Net with a PSE Structure. *Remote Sens.* **2019**, *11*, 2053. [[CrossRef](#)]
- Zhang, Y.; Wang, C.; Ji, Y.; Chen, J.; Deng, Y.; Chen, J.; Jie, Y. Combining Segmentation Network and Nonsampled Contourlet Transform for Automatic Marine Raft Aquaculture Area Extraction from Sentinel-1 Images. *Remote Sens.* **2020**, *12*, 4182. [[CrossRef](#)]
- Skirtun, M.; Sandra, M.; Strietman, W.J.; van den Burg, S.W.; De Raedemaeker, F.; Devriese, L.I. Plastic pollution pathways from marine aquaculture practices and potential solutions for the North-East Atlantic region. *Mar. Pollut. Bull.* **2022**, *174*, 113178. [[CrossRef](#)]
- Gao, X.; Zhou, F.; Chen, C.-T.A. Pollution status of the Bohai Sea: An overview of the environmental quality assessment related trace metals. *Environ. Int.* **2014**, *62*, 12–30. [[CrossRef](#)]
- Liu, F.; Pang, S.; Chopin, T.; Gao, S.; Shan, T.; Zhao, X.; Li, J. Understanding the recurrent large-scale green tide in the Yellow Sea: Temporal and spatial correlations between multiple geographical, aquacultural and biological factors. *Mar. Environ. Res.* **2013**, *83*, 38–47. [[CrossRef](#)] [[PubMed](#)]
- Gao, H.; Zhou, J.; Dong, S.; Kitazawa, D. Sustainability Assessment of Marine Aquaculture considering Nutrients Inflow from the Land in Kyushu Area. *Water* **2022**, *14*, 943. [[CrossRef](#)]
- He, N.; Liu, L.; Wei, R.; Sun, K. Heavy Metal Pollution and Potential Ecological Risk Assessment in a Typical Mariculture Area in Western Guangdong. *Int. J. Environ. Res. Public Health* **2021**, *18*, 11245. [[CrossRef](#)] [[PubMed](#)]
- Xu, G.; Shen, W.; Wang, X. Applications of Wireless Sensor Networks in Marine Environment Monitoring: A Survey. *Sensors* **2014**, *14*, 16932–16954. [[CrossRef](#)] [[PubMed](#)]
- Romieu, E.; Welle, T.; Schneiderbauer, S.; Pelling, M.; Vinchon, C. Vulnerability assessment within climate change and natural hazard contexts: Revealing gaps and synergies through coastal applications. *Sustain. Sci.* **2010**, *5*, 159–170. [[CrossRef](#)]
- Hou, X.Y.; Xu, X.L. Spatial patterns of land use in coastal zones of China in the early 21st century. *Geogr. Res.* **2011**, *30*, 1370–1379.
- Liang, C.; Cheng, B.; Xiao, B.; He, C.; Liu, X.; Jia, N.; Chen, J. Semi-/Weakly-Supervised Semantic Segmentation Method and Its Application for Coastal Aquaculture Areas Based on Multi-Source Remote Sensing Images—Taking the Fujian Coastal Area (Mainly Sanduo) as an Example. *Remote Sens.* **2021**, *13*, 1083. [[CrossRef](#)]
- Wong, B.A.; Thomas, C.; Halpin, P. Automating offshore infrastructure extractions using synthetic aperture radar & Google Earth Engine. *Remote Sens. Environ.* **2019**, *233*, 111412.
- Wang, J.; Yang, X.; Wang, Z.; Ge, D.; Kang, J. Monitoring Marine Aquaculture and Implications for Marine Spatial Planning—An Example from Shandong Province, China. *Remote Sens.* **2022**, *14*, 732. [[CrossRef](#)]
- Zhang, X.; Xiao, P.; Feng, X. Object-specific optimization of hierarchical multiscale segmentations for high-spatial resolution remote sensing images. *ISPRS J. Photogramm. Remote Sens.* **2020**, *159*, 308–321. [[CrossRef](#)]
- Jiang, Z.; Ma, Y. Accurate extraction of offshore raft aquaculture areas based on a 3D-CNN model. *Int. J. Remote Sens.* **2020**, *41*, 5457–5481. [[CrossRef](#)]
- Wang, M.; Cui, Q.; Wang, J.; Ming, D.; Lv, G. Raft cultivation area extraction from high resolution remote sensing imagery by fusing multi-scale region-line primitive association features. *ISPRS J. Photogramm. Remote Sens.* **2017**, *123*, 104–113. [[CrossRef](#)]
- Cheng, B.; Liang, C.; Liu, X.; Liu, Y.; Wang, G. Research on a novel extraction method using Deep Learning based on GF-2 images for aquaculture areas. *Int. J. Remote Sens.* **2020**, *41*, 3575–3591. [[CrossRef](#)]
- Wang, J.; Sui, L.; Yang, X.; Wang, Z.; Liu, Y.; Kang, J.; Lu, C.; Yang, F.; Liu, B. Extracting Coastal Raft Aquaculture Data from Landsat 8 OLI Imagery. *Sensors* **2019**, *19*, 1221. [[CrossRef](#)]
- Liu, Y.; Wang, Z.; Yang, X.; Zhang, Y.; Cai, P. Satellite-based monitoring and statistics for raft and cage aquaculture in China's offshore waters. *Int. J. Appl. Earth Obs. Geoinf.* **2020**, *91*, 102118. [[CrossRef](#)]

26. Lu, X.; Zhang, Y.; Zhang, S.; Li, Y. Spatial Change Analysis of *Porphyra yezoensis* Aquaculture in the Lianyungang Coastal Area by the Use of Remote Sensing and Geographic Information System Technology. *J. Indian Soc. Remote Sens.* **2019**, *47*, 1609–1622. [[CrossRef](#)]
27. Liu, Y.; Yang, X.; Wang, Z.; Lu, C.J. Extracting raft aquaculture areas in Sanduao from high-resolution remote sensing images using RCF. *Acta Oceanol. Sin.* **2019**, *41*, 119–130.
28. Fu, Y.; Deng, J.; Wang, H.; Comber, A.; Yang, W.; Wu, W.; You, S.; Lin, Y.; Wang, K. A new satellite-derived dataset for marine aquaculture areas in China's coastal region. *Earth Syst. Sci. Data* **2021**, *13*, 1829–1842. [[CrossRef](#)]
29. Fu, Y.; Ye, Z.; Deng, J.; Zheng, X.; Wang, K. Finer Resolution Mapping of Marine Aquaculture Areas Using WorldView-2 Imagery and a Hierarchical Cascade Convolutional Neural Network. *Remote Sens.* **2019**, *11*, 1678. [[CrossRef](#)]
30. The State of world fisheries and aquaculture, 2012. *Choice Rev. Online* **2013**, *50*, 50-5350.
31. Felde, G.W.; Anderson, G.P.; Cooley, T.W.; Matthew, M.W.; Lee, J. Analysis of Hyperion Data with the FLAASH Atmospheric Correction Algorithm. In Proceedings of the 2003 IEEE International Geoscience and Remote Sensing Symposium (IGARSS 2003), Toulouse, France, 21–25 July 2003.
32. Kaplan, G.; Avdan, U. Object-based water body extraction model using Sentinel-2 satellite imagery. *Eur. J. Remote Sens.* **2017**, *50*, 137–143. [[CrossRef](#)]
33. Wang, Z.; Yang, X.; Liu, Y.; Lu, C. Extraction of coastal raft cultivation area with heterogeneous water background by thresholding object-based visually salient NDVI from high spatial resolution imagery. *Remote Sens. Lett.* **2018**, *9*, 839–846. [[CrossRef](#)]
34. Szeliski, R. *Computer Vision: Algorithms and Applications*; Springer: Berlin/Heidelberg, Germany, 2011.
35. Bradski, G.; Kaehler, A. *Learning OpenCV: Computer Vision with the OpenCV Library*; O'Reilly Media, Inc.: Sebastopol, CA, USA, 2008.
36. Canny, J. A Computational Approach to Edge Detection. *IEEE Trans. Pattern Anal. Mach. Intell.* **1986**, *PAMI-8*, 679–698. [[CrossRef](#)]
37. Roth, S.; Leiterer, R.; Volpi, M.; Celio, E.; Schaepman, M.E.; Joerg, P.C. Automated detection of individual clove trees for yield quantification in northeastern Madagascar based on multi-spectral satellite data. *Remote Sens. Environ.* **2018**, *221*, 144–156. [[CrossRef](#)]
38. Lapušinskij, A.; Suzdalev, I.; Goranin, N.; Janulevičius, J.; Ramanauskaitė, S.; Stankūnavičius, G. The Application of Hough Transform and Canny Edge Detector Methods for the Visual Detection of Cumuliform Clouds. *Sensors* **2021**, *21*, 5821. [[CrossRef](#)]
39. Varun, R.; Kini, Y.V.; Manikantan, K.; Ramachandran, S. Face Recognition Using Hough Transform Based Feature Extraction. *Procedia Comput.* **2015**, *46*, 1491–1500. [[CrossRef](#)]
40. Berendes, T.; Sengupta, S.K.; Welch, R.M.; Wielicki, B.A.; Navar, M. Cumulus cloud base height estimation from high spatial resolution Landsat data: A Hough transform approach. *IEEE Trans. Geosci. Remote Sens.* **1992**, *30*, 430–443. [[CrossRef](#)]
41. Rizon, M.; Yazid, H.; Saad, P.; Shakaff, A.Y.M.; Saad, A.R.; Sugisaka, M.; Yaacob, S.; Mamat, M.R.; Karthigayan, M. Object Detection Using Circular Hough Transform. *Am. J. Appl. Sci.* **2005**, *2*, 1606–1609. [[CrossRef](#)]
42. Xu, Z.; Qian, C. A novel method for circular objects extraction based on region information. *Signal Image Video Process.* **2022**, *16*, 523–531. [[CrossRef](#)]
43. Liu, Y.; Sun, C.; Yang, Y.; Zhou, M.; Zhan, W.; Cheng, W. Automatic extraction of offshore platforms using time-series Landsat-8 Operational Land Imager data. *Remote Sens. Environ.* **2016**, *175*, 73–91. [[CrossRef](#)]
44. Lu, Y.; Shao, W.; Sun, J. Extraction of Offshore Aquaculture Areas from Medium-Resolution Remote Sensing Images Based on Deep Learning. *Remote Sens.* **2021**, *13*, 3854. [[CrossRef](#)]
45. Virdis, S.G.P. An object-based image analysis approach for aquaculture ponds precise mapping and monitoring: A case study of Tam Giang-Cau Hai Lagoon, Vietnam. *Environ. Monit Assess.* **2014**, *186*, 117–133. [[CrossRef](#)] [[PubMed](#)]
46. Zhou, W.; Wang, F.; Wang, X.; Tang, F.; Li, J. Evaluation of Multi-Source High-Resolution Remote Sensing Image Fusion in Aquaculture Areas. *Appl. Sci.* **2022**, *12*, 1170. [[CrossRef](#)]
47. Chen, G.; Weng, Q.; Hay, G.J.; He, Y. Geographic object-based image analysis (GEOBIA): Emerging trends and future opportunities. *GISci Remote Sens.* **2018**, *55*, 159–182. [[CrossRef](#)]